Effect of milling on the electrical properties of Ba(Fe$_{1/2}$Ta$_{1/2}$)O$_3$ ceramic

Uttam K. Mahto[1a], Sumit K. Roy[2b], S. Chaudhuri[2c] and K. Prasad[*1,3]

[1]*Aryabhatta Centre for Nanoscience and Nanotechnology, Aryabhatta Knowledge University, Patna 800001, India*
[2]*Department of Physics, St. Xavier's College, Ranchi 834001, India*
[3]*University Department of Physics, T.M. Bhagalpur University, Bhagalpur 812 007, India*

Abstract. In this work effect of high energy milling on the structural and electrical properties of Ba(Fe$_{1/2}$Ta$_{1/2}$)O$_3$ (BFT) ceramic synthesized using standard solid-state reaction method were investigated. X-ray diffraction studies indicated that the unit cell structure for all the samples to be hexagonal (space group: *P3m*1). FTIR spectra also confirmed the formation of BFT without any new phase. The milled (10 h) BFT ceramic showed the formation of small grain sizes (<2 μm) which is beneficial for dielectric applications in high density integrated devices. Besides, the milled (10 h) BFT ceramic sample exhibited superior dielectric properties (enhancement in ε'-value and reduction in tgδ - value) compared to un-milled one. Impedance analysis indicated the negative temperature coefficient of resistance (NTCR) character. The correlated barrier hopping model (jump relaxation type) is found to successfully explain the mechanism of charge transport in present ceramic samples.

Keywords: Ba(Fe$_{1/2}$Ta$_{1/2}$)O$_3$; lead-free; structure; perovskite; dielectric constant; FTIR spectroscopy; electroceramic

1. Introduction

Complex perovskites with general formula A(B$'_{1/2}$B$''_{1/2}$)O$_3$ exhibiting very high dielectric constant (ε>10^3) are of technological importance as they find their applications in different electronic and/or microelectronic devices especially in capacitors, sensors, actuators, memory devices, power transmission, high energy storage, etc. Most of the perovskite type materials, showing high dielectric constant, generally contain lead which inevitably causes environmental pollution due to the toxicity of lead oxide and are not recyclable. It is, therefore, necessary to search alternative lead-free compounds for such applications, which should have either comparable or superior dielectric properties. It is observed that complex lead-free perovskite such

---

∗Corresponding author, Professor, E-mail: k.prasad65@gmail.com
[a]M.Tech., E-mail: uttam_astam@rediffmail.com
[b]Ph.D. Student and Faculty, E-mail: sumit.sxc13@gmail.com
[c]Faculty, E-mail: joyranchi@yahoo.com

as $Ba(Fe_{1/2}Nb_{1/2})O_3$ (Raevski *et al.* 2003, Chung *et al.* 2004, Wang *et al.* 2007a, Intatha *et al.* 2010, Bhagat and Prasad 2010, Ke *et al.* 2013, Patel *et al.* 2014, Bhagat *et al.* 2014, Bochenek *et al.* 2015), $Ba(Bi_{1/2}Nb_{1/2})O_3$ (Prasad *et al.* 2009, Prasad *et al.* 2010a), $Ba(Al_{1/2}Nb_{1/2})O_3$ (Dutta and Sinha 2006, Prasad *et al.* 2010b), $Sr(Fe_{1/2}Nb_{1/2})O_3$ (Raevski *et al.* 2003), $Ba(Fe_{1/2}Ta_{1/2})O_3$ (Jung *et al.* 2002, Li *et al.* 2004a, Wang *et al.* 2007b, Phatungthane *et al.* 2014), $Ba(Bi_{1/2}Ta_{1/2})O_3$ (Mishra *et al.* 2012), etc. ceramics exhibit giant dielectric constant. Among these, $Ba(Fe_{1/2}Ta_{1/2})O_3$ (abbreviated hereafter as BFT) is an $A(B'_{1/2}B''_{1/2})O_3$ complex perovskite, where B' and B'' are cations of different valencies at the B-site. Galasso *et al.* (1959) reported that the crystal structure of BFT to be cubic and showed ferroelectric properties even though it has a cubic perovskite structure. In another report, Agranovskaya (1960) showed ambiguous dielectric characteristic of BFT with a large dielectric loss tangent (>1). Later on, a detailed crystal structure analysis was carried out and illustrated that BFT had a cubic symmetry which cannot possess ferroelectric properties even though the presence of disordered cations at B-site (Galasso and Darby 1962). Besides, Li *et al.* (2004a) showed the true symmetry of BFT to be trigonal with space group of $P3m1$ on the basis transmission electron microscope micrograph and Mössbauer spectrum studies. Further, new lead-free materials with recent technologies leading to higher efficiency and miniaturization have opened up scope for the development of highly integrated devices. To this end, large grain sizes (>3 μm) and high dissipation factor such materials poses difficulty in developing a dielectric layer less than 10 μm with higher capacitance values. Accordingly, in the present work, $Ba(Fe_{1/2}Ta_{1/2})O_3$ ceramic was prepared be a standard solid state reaction (industrially viable method) technique and its fine powder was obtained using high energy ball milling method. The BFT ceramic as well as nanoceramic were characterized using structural (X-ray and its Rietveld analysis), microstructural, infrared spectroscopy (IR), dielectric, impedance and ac conductivity studies.

2. Materials and methods

2.1 Preparation of ceramic and nanoceramic samples

The polycrystalline sample of $Ba(Fe_{1/2}Ta_{1/2})O_3$ was prepared by the conventional solid-state reaction method and its fine powder was obtained using a high energy ball milling technique (Fig. 1). High purity (>99.5%, Alfa Aesar, USA) carbonates/oxides of $BaCO_3$, Fe_2O_3 and Ta_2O_5 were mixed in proper stoichiometry. Wet mixing was carried out in an acetone medium for homogeneous mixing. Grinding was performed using pestle and mortar for about 2 h. Well-mixed powders were then calcined at 1300°C/4 h using an alumina crucible in a high temperature furnace (Nabertherm, Germany). The completion of reaction and the formation of desired compound were checked by X-ray diffraction technique. The as-calcined powder was subjected to a bench top grinding machine (Retsch PM 200, Germany) at room temperature. The milling process was performed with tungsten carbide (WC) vial and WC balls of 10 mm diameter at a speed of 300 rpm with the ball-to-powder weight ratio of 30:1. The milled fine powders were taken out at different milling time (2.5 h, 5 h, 7.5 h and 10 h) for their structural and IR analysis. Further, the calcined (un-milled) and milled (10 h) powders were compacted into thin (~1.25 mm) circular disks with an applied uniaxial pressure of 650 MPa. The pellets were sintered in air atmosphere, respectively, at 1325°C/3 h and 1250°C/2 h for un-milled and milled BFT samples.
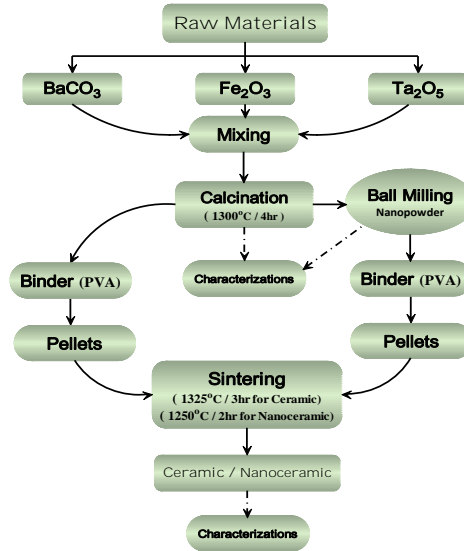
Fig. 1 Schematics for the synthesis of Ba(Fe$_{1/2}$Ta$_{1/2}$)O$_3$ ceramic and nanoceramic

2.2 Characterizations

The XRD data of un-milled and milled (2.5 h, 5 h, 7.5 h and 10 h) powders were obtained with an X-ray diffractometer (XPERT-PRO, Pan Analytical) at room temperature, using CuK$_\alpha$ radiation (λ=1.5405 Å) over a wide range of Bragg angles (20°≤2θ≤80°) with a scanning speed of 5.08° min^{-1}. The dimensions of the unit cell, *hkl* values and space group of all the specimens were obtained using an X'Pert Highscore Plus software. The Fourier transformed infrared (FTIR) spectra of all the samples were collected in the transmission mode using an Alpha-T Bruker FTIR spectrophotometer in the range of 500-5000 cm^{-1}. The scanning electron micrographs (SEM) of un-milled and milled (10 h) samples were collected using a using an HR-SEM (FEI Quanta FEG 200). Dielectric and impedance measurements were carried out as function of frequency (20 Hz - 1 MHz) at different temperatures (20°C - 400°C) using a computer-interfaced Impedance analyzer (E4990A-120, Keysight Technologies, USA). AC conductivity data were thus obtained using the relation: $\sigma_{ac} = 2\pi f \varepsilon_o \varepsilon \tan \delta$; where *f*, ε, and tanδ are operating frequency, dielectric constant and loss tangent respectively.

3. Results and discussion

X-ray diffraction patterns of un-milled and milled (2.5 h, 5 h, 7.5 h and 10 h) ceramic powders along with their Rietveld refinement profiles are depicted in Fig. 2. All the compounds show a single hexagonal phase formation with space group *P3m*1. The refined unit cell parameters are listed in Table 1. This lattice information obtained in the present work is in consistent with the earlier report (Li *et al*. 2004a). A careful look at the XRD peaks (Fig. 2) suggested that the mechanical alloying led to a significant broadening of XRD peaks indicating the reduction in particle sizes of BFT. The increase in peak width indicated the formation of fine grain and a high
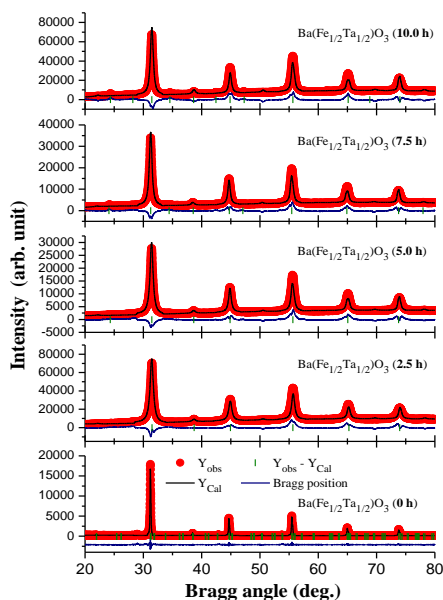
Fig. 2 X-ray diffraction patterns of Ba(Fe$_{1/2}$Ta$_{1/2}$)O$_3$ ceramic powders at different milling times

Table 1 The lattice parameters of un-milled and milled Ba(Fe$_{1/2}$Ta$_{1/2}$)O$_3$ obtained from X-ray powder diffraction data at different milling times

Parameters	0 hr *un-milled*	2.5 hrs *milled*	5.0 hrs *milled*	7.5 hrs *milled*	10.0 hrs *milled*
Crystal System	Hexagonal	Hexagonal	Hexagonal	Hexagonal	Hexagonal
Space group	*P3m*1	*P3m*1	*P3m*1	*P3m*1	*P3m*1
a (Å)	5.740	5.741	5.765	5.764	5.765
b (Å)	5.740	5.741	5.765	5.764	5.765
c (Å)	14.058	14.063	14.033	14.034	14.027

density of defects caused by a large local strain in the powder particles (Giri *et al*. 2007, Sivasankaran *et al*. 2011, Rebuffi *et al*. 2016). The XRD patterns also reveals that the peak intensities increase with increase of milling time, suggesting the compressive strain in milled samples and more change along the *c*-direction (Giri *et al*. 2007, Deepika *et al*. 2014).

Fig. 3 shows the FTIR spectra of all un-milled and milled samples in the mid infrared region. The formation of a perovskite structure can be confirmed by the presence of multiple metal-oxygen (M-O) band between 1015 cm^{-1} to 1433 cm^{-1} (Lee *et al*. 2005, Li *et al*. 2004b). Strong absorptive peak at 587 cm^{-1} may be attributed to the Fe-O stretching and bending vibration which is characteristic of octahedral FeO$_6$ groups in the perovskite compounds (Sahoo *et al*. 2010), which get broadened with increasing milling hour, may be due to particle size reduction. All the samples contain weak band at 2848 cm^{-1} -2928 cm^{-1} which corresponds to carbonate groups, may be due to atmospheric CO$_2$. The bands at 1639 cm^{-1} and 3442 cm^{-1} are assigned to the bending of H-O-H and O-H stretching modes of vibration due to physically adsorbed water molecules on the surface of the sample during palletization with KBr for all the cases.
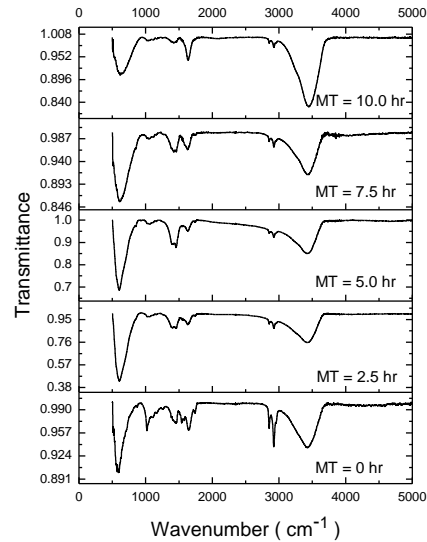
Fig. 3 FTIR spectra of Ba(Fe$_{1/2}$Ta$_{1/2}$)O$_3$ ceramic powders at different milling times
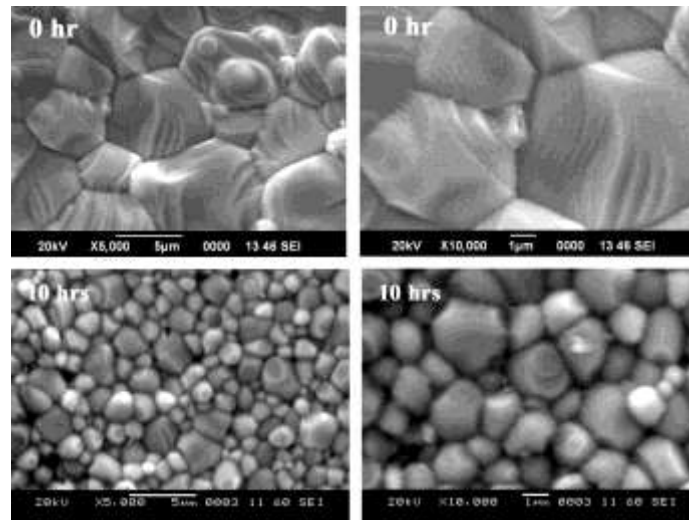

Fig. 4 SEM image of un-milled and milled (10 h) Ba(Fe$_{1/2}$Ta$_{1/2}$)O$_3$ ceramic

Fig. 4 displays the SEM micrographs of fractured surface of sintered BFT un-milled and milled (10 h) ceramics. The nature of the micrographs clearly exhibits the polycrystalline texture of the materials and grains are distributed throughout the samples and are almost free from any pores or voids, suggesting the high density of the materials. The micrographs clearly show a sharp reduction in the average grain size from ~4 μm (for un-milled BFT sample) to ~1.5 μm (for 10 h milled BFT sample). This may be due to the reduction in particle sizes which might have produced some stress during high energy milling (Deepika *et al*. 2014). This generated stress could prevent grain boundary movement during the sintering and thereby resulted in the reduction of grain size.
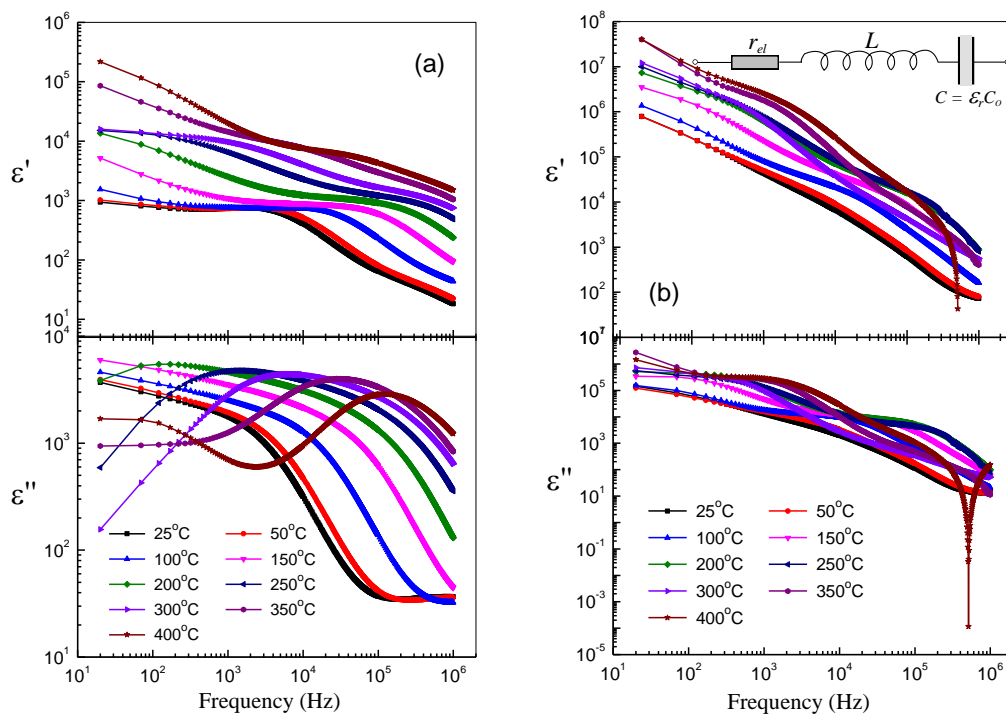
Fig. 5 Frequency dependence of real and imaginary parts of dielectric constant of (a) un-milled and (b) 10 h milled Ba(Fe$_{1/2}$Ta$_{1/2}$)O$_3$ ceramics at different temperatures. Inset: Capacitor model described for frequency of operation

Furthermore, as known, sintering is the process of compacting and forming a solid mass of material by heat energy or mechanical pressure without melting it to the point of liquefaction. The significant difference in sintering temperature of the un-milled and 10 h milled samples can be attributed to the fact that during milling, energy is supplied to the powder samples in the form of mechanical energy which reduces the melting point of the material with lowering of particle sizes and so less heat energy (sintering temperature/duration) is required for sintering of milled samples (Kong *et al.* 2008).

The frequency response of the real, $\varepsilon'(f)$ and imaginary, $\varepsilon''(f)$, parts of permittivity data at different temperatures, are shown in Fig. 5(a) un-milled and (b) milled (10 h) BFT ceramic samples. It is observed that both ε' and ε'' follows inverse dependence on frequency for both the cases which is due to the fact that dipoles can no longer follow the field at high frequencies. The major contribution in low frequency region is due to the ionic polarizability, whereas in the high frequency region the effect of electronic polarizability becomes dominant (Gergs *et al.* 2007, Tickoo *et al.* 2003). All samples show dielectric dispersion with frequency in the lower frequency region. This can be explained due to Maxwell-Wagner type interfacial polarization in agreement with Koop's phenomenological theory (Tickoo 1951). Besides, it is observed that a peak starts appearing in the ε''-f plots which shifts to higher frequencies when temperature is increased with a decrease in its amplitude (Fig. 5). Also, ε'-f as well as ε''-f plots find a minimum at 400°C for

milled (10 h) sample, which may be due to the resonance effect (Bhagat and Prasad 2010) where the real part of the permittivity becomes negative at the resonance frequency. It is known that the resonance effect places an upper limit on the frequency at which the capacitor can normally be used. Above the self-resonant frequency the capacitor behaves as a DC blocking inductor and the permittivity becomes negative since the inductive reactance (ωL) predominates over the capacitive reactance and this is significant for some applications e.g., ceramic multilayer capacitors are commonly used to decouple high-speed computer circuits, with a prime function is to eliminate noise which has frequency components above the resonance frequency. Therefore the inductive reactance should be kept as small as possible. Inset of Fig. 5(b) shows equivalent circuit in such a case, where both resistance and impedance of the measuring setup influence detected dielectric response. Complex impedance of such equivalent circuit shall be: $Z = r_{el} + j\omega L - j/\omega C^{*}$. Here r_{el} and L are the resistance and inductance of the leads and electrodes.

Fig. 6(a) and (b), respectively show the temperature dependence of the ε' and ε'' at different frequencies for un-milled and milled (10 h) BFT ceramic samples. The ε'-T curves for un-milled sample presented a step-like dielectric constant with high values of dielectric constant over a wide temperature range (upto ~300°C), especially at low frequency thereafter it starts increasing. This behavior is similar to those reported in previous works in BFT ceramics (Li *et al.* 2004a, Wang *et al.* 2007b). Similar behaviour with higher values of ε' is observed in case of milled sample except that ε'-T curves find a peak at 225°C which shifts toward higher
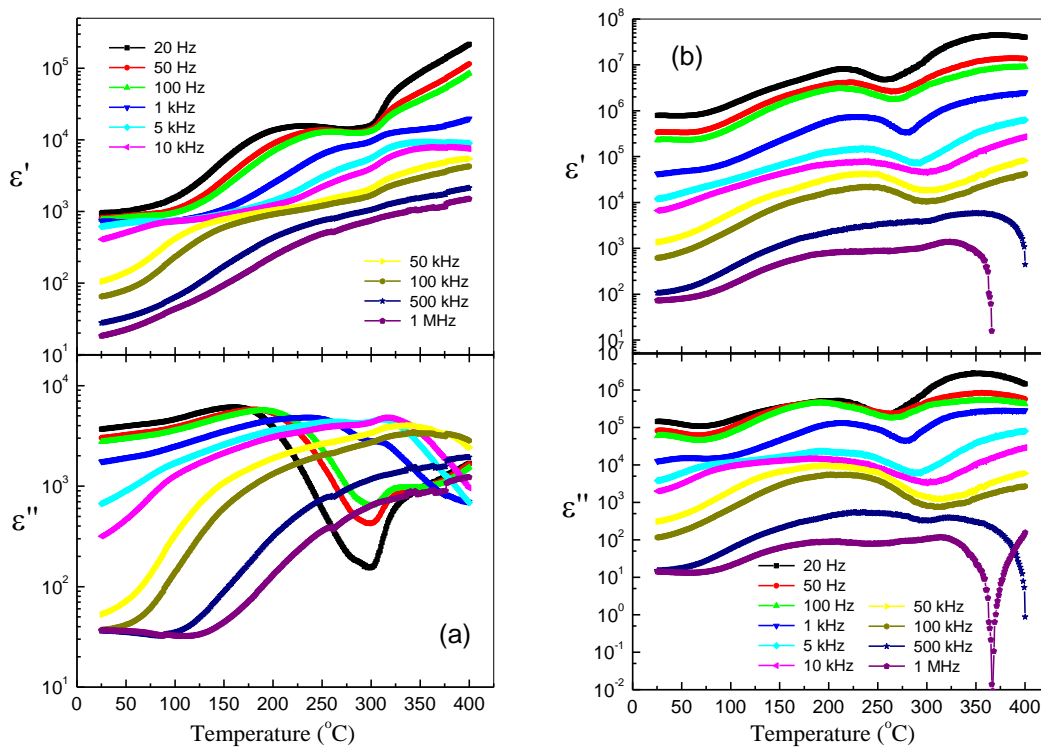

Fig. 6 Temperature dependence of real and imaginary parts of dielectric constant of (a) un-milled and (b) 10 h milled Ba(Fe$_{1/2}$Ta$_{1/2}$)O$_3$ ceramics at different frequencies

temperature side with increasing frequency. The ε''-T curves show a single peak which shifts toward higher temperature side with increasing frequency in both the cases. Furthermore, the resonance effect could be seen for milled (10 h) sample in ε'-T and ε''-T plots at higher temperatures and frequencies $\geq$500 kHz (Fig. 6(b)). The values of ε' and ε'' at 25°C are respectively found to be 740 and 1782 for un-milled and 44126 and 13147 for milled (10 h) BFT ceramic samples at 1 kHz. The reason for the high dielectric constant could be considered due to the grain-boundary and/or the grain-size dependent extrinsic factors as well as a significant contribution of the intrinsic factors related to chemical substitution induced localized electronic structure modifications might plays a crucial role. Hence, 10 h milled BFT ceramic sample exhibits drastically superior dielectric properties (enhancement in ε'-value and reduction in tgδ ($=\varepsilon''/\varepsilon'$=0.30) value) compared to un-milled one. Therefore, milled (10 h) BFT ceramic with small grain sizes ($<$2 μm) could be considered as a potential lead-free candidate for dielectric applications in high density integrated devices.

The logarithmic frequency dependence of real (Z') and imaginary (Z'') parts of impedance of un-milled and 10 h milled BFT samples, at different temperatures are plotted in Figs. 7(a) and (b), respectively. It is observed that the values of Z' decreases with increasing frequency as well as temperature in both the cases. This indicates the negative temperature coefficient of resistance (NTCR) character of BFT ceramics. Further, at lower temperatures, the values of Z'' decrease monotonically suggesting the absence of any relaxation. This suggests that the relaxation
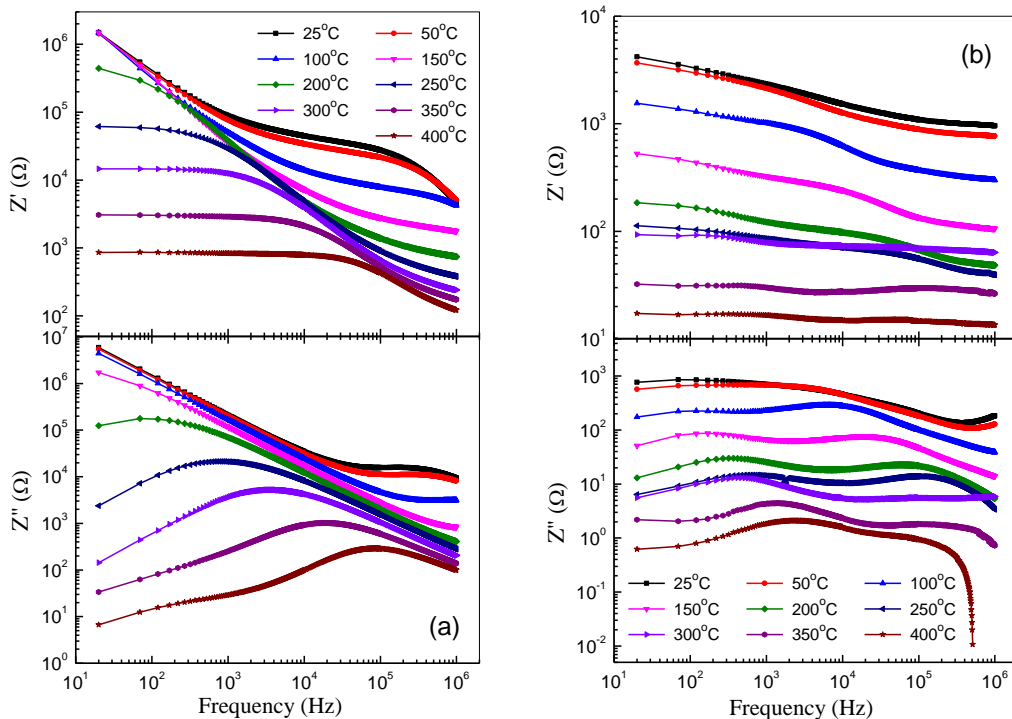

Fig. 7 Frequency dependence of real and imaginary parts of impedance of (a) un-milled and (b) 10 h milled Ba(Fe$_{1/2}$Ta$_{1/2}$)O$_3$ ceramics at different temperatures
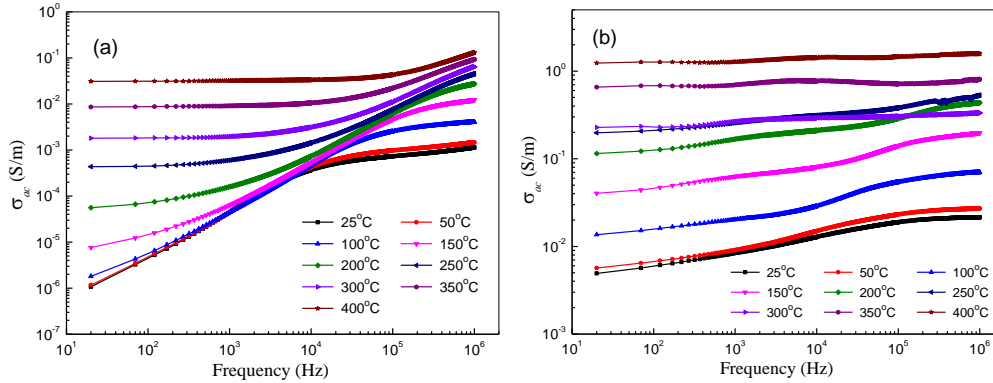
Fig. 8 Frequency dependence of ac conductivity of (a) un-milled and (b) 10 h milled Ba(Fe$_{1/2}$Ta$_{1/2}$)O$_3$ ceramics at different temperatures

species are immobile defects and the orientation effect might be associated. As the temperature increases, the peak in Z''-f plots starts appearing, which shifts towards higher frequency side with the increment in temperature showing the resistance of the bulk material is decreasing and supports NTCR character of un-milled and milled BFT. Upon further rise in temperature Z''-f plots exhibited double peaks (400°C in case of un-milled and 150°C in case of milled BFT samples), which clearly indicated the introduction of grain boundary effect. Besides the magnitude of Z'' peaks decreases while the width of the peak increases with increasing temperature and the peaks are slightly asymmetric in nature for both the samples, which suggests that there is a spread of relaxation times i.e. the existence of a temperature dependent electrical relaxation in the materials (Prasad *et al*. 2007a).

Figs. 8(a) and (b), respectively show the log-log plots of ac electrical conductivity versus frequency at different temperatures for un-milled and 10 h milled BFT ceramics. Both the samples exhibit three different conductivity regions: (i) low frequency plateau, (ii) mid frequency dispersion and (iii) high frequency plateau. The low frequency plateau is due to the dc conductivity originating from the free charge carriers. Apart from the plateau, low frequency dispersion is also observed, indicating an apparent ac conductivity contribution even in low frequency region. This may be due to the absence of free charges required for dc conduction in the system. The observed strong dispersion at mid frequency and the plateau at the high frequency are related to the ac conductivity. In order to understand the mechanism of conduction process, ac conductivity data were analysed using the modified power law (Tiwari and Shahi 2007): $\sigma_{ac} = \sigma_o \omega^{S_o} + A_1 \omega^{S_1} + A_2 \omega^{S_2}$. The first term on the right hand side of equation indicates the dc conductivity (s_o=0) as observed in the low frequency region. The second and third terms represent the mid frequency *strong* dispersion (s_1) and the high frequency *weak* dispersion (plateau s_2≈0), respectively. The values of the s parameter are obtained using the derivative equation: s=d lnσ_{ac}/d lnω. A_1 and A_2 are the temperature dependent constants. A non-zero value of the index s_o at low frequencies is observed due to the low frequency dispersion which results from the long-range translational motion of the conducting charge carriers (i.e., induced electrons). In the mid frequency region, value of index increases rapidly and after reaching a peak, it becomes nearly linear at higher frequencies. The value of s_1 parameter is found to be greater than unity while the values of the s_2 parameter are close to zero. The observed nature of s in various frequency regions

can be successfully explained on the basis of hopping of ions (Funke 1993, Funke 1994). As the input ac frequency increases, the rate of successful hopping, indicated by the frequency exponent *s*, increases. The conductivity in this region corresponds to the short-range translational hopping related to forward-backward jump. The peak position (mid frequency) represents a condition where the number of successful and unsuccessful attempts becomes nearly equal. Beyond this region, the number of carriers (dipoles/oxygen vacancies) available for hopping gradually reaches saturation. This leads to a reduction of the frequency exponent *s*. The high frequency plateau, indicated as s_2, corresponds to a saturation region of charge carriers undergoing relaxational hopping. Therefore, Jump Relaxation Model (Tiwari and Shahi 2007) successfully described the contribution of the free charges, induced space charges, and the oxygen vacancy induced dipoles in the measured frequency range for both the samples. Furthermore, it is observed that the hopping conduction mechanism is generally consistent with the existence of a high density of states in the materials having band gap like that of semiconductor. Due to localization of charge carriers, formation of polarons takes place and the hopping conduction may occur between the nearest neighboring sites. The values of E_a (apparent activation energy of conduction) were estimated for both un-milled and 10 h milled BFT samples using a linear least square fitting method and the Arrhenius relationship: $\sigma_{ac} = \sigma_o + \exp(-E_a/k_B T)$, respectively, to be 0.018 eV and 0.098 eV at 1 kHz. The low value of E_a may be due to the carrier transport through hopping between localized states in a disordered manner (Prasad *et al*. 2007b).

4. Conclusions

Polycrystalline $Ba(Fe_{1/2}Ta_{1/2})O_3$ ceramic, prepared by a high temperature solid-state reaction route and its high energy milling was carried out with different milling hours. The un-milled as well as milled ceramic were found to possess a perovskite type hexagonal structure with the space group *P*3*m*1. FTIR spectra also confirmed the formation of BFT without any new phase. The milled (10 h) BFT ceramic showed the formation of small grain sizes ($<2\ \mu$m) which is beneficial for dielectric applications in high density integrated devices. Also, the milled (10 h) BFT ceramic sample exhibited superior dielectric properties (enhancement in ε'-value and reduction in tgδ-value) compared to un-milled one. Impedance analysis indicated the negative temperature coefficient of resistance (NTCR) character. The correlated barrier hopping model (jump relaxation type) is found to successfully explain the mechanism of charge transport in present ceramic system.

Acknowledgments

References

Agranovskaya, A.I. (1960), "Physical-chemical investigation of the formation of complex ferroelectrics with the perovskite structure", *Bull. Acad. Sci. USSR, Phys. Ser*., **24**, 1271-1277.

Bhagat, S., AmarNath, K., Chandra, K.P., Singh, R.K., Kulkarni, A.R. and Prasad, K. (2014), "The structural, electrical and magnetic properties of perovskite (1-x)Ba(Fe$_{1/2}$Nb$_{1/2}$)O$_3$-xBaTiO$_3$ ceramics", *Adv. Mater. Lett.*, **5**, 117-121.

Bhagat, S. and Prasad, K. (2010), "Structural and impedance spectroscopy analysis of Ba(Fe$_{1/2}$Nb$_{1/2}$)O$_3$ ceramic", *Phys. Status Solidi A*, **207**(5), 1232-1239.

Bochenek, D., Niemiec, P., Szafraniak-Wiza, I., Adamczyk, M. and Skulski, R. (2015), "Preparation and dielectric properties of the lead-free BaFe$_{1/2}$Nb$_{1/2}$O$_3$ ceramics obtained from mechanically triggered powder", *Eur. Phys. J. B*, **88**(10), 277-281.

Chung, C.-Y., Chang, Y.-H. and Chen, G.-J. (2004), "Effects of lanthanum doping on the dielectric properties of Ba(Fe$_{0.5}$Nb$_{0.5}$)O$_3$ ceramic", *J. Appl. Phys.*, **96**(11), 6624-6628.

Dutta, A. and Sinha, T.P. (2006), "Dielectric relaxation in Perovskite Ba(Al$_{1/2}$Nb$_{1/2}$)O$_3$", *J. Phys. Chem. Solids*, **67**(7), 1484-1491.

Deepika, Li, L.H., Glushenkov, A.M., Hait, S.K., Hodgson, P. and Chen, Y. (2014), "High-efficient production of boron nitride nanosheets via an optimized ball milling process for lubrication in oil", *Sci. Rep.*, **4**, 7288-7293.

Funke, K. (1993), "Jump relaxation in solid electrolytes", *Prog. Solid St. Chem.*, **22**(2), 111-115.

Funke, K. (1994), "Jump relaxation model and coupling model - a comparison", *J. Non-Cryst. Solids*, **172-174**, 1215-1221.

Galasso, F. and Darby, W. (1962), "Ordering of the octahedrally coordinated cation position in the perovskite structure", *J. Phys. Chem.*, **66**(1), 131-132.

Galasso, F., Katz, L. and Ward, R. (1959), "Substitution in the octahedrally coordinated cation positions in compounds of the perovskite type", *J. Am. Chem. Soc.*, **81**(4), 820-823.

Gergs, M., Gamal, G. and Massaud, M. (2007), "Dielectric properties, Deby relaxation time and activation energy of [(Pb$_{1-x}$Sr$_x$)$_{1-1.5z}$La$_z$]TiO$_3$ ceramics", *Egypt. J. Solid*, **30**, 20-35.

Giri, P., Bhattacharyya, S., Singh, D.K., Kesavamoorthy, R., Panigrahi, B.K. and Nair, K.G.M. (2007), "Correlation between microstructure and optical properties of ZnO nanoparticles synthesized by ball milling", *J. Appl. Phys.*, **102**(9), 093515-8.

Intatha, U., Eitssayeam, S., Wang, J. and Tunkasiri, T. (2010), "Impedance study of giant dielectric permittivity in BaFe$_{0.5}$Nb$_{0.5}$O$_3$ perovskite ceramic", *Curr. Appl. Phys.*, **10**(1), 21-25.

Jung, W.-H., Lee, J.-H., Sohn, J.-H., Nam, H.-D. and Cho, S.-H. (2002), "Dielectric loss anomaly in Ba(Fe$_{1/2}$Ta$_{1/2}$)O$_3$ ceramics", *Mater. Lett.*, **56**(3), 334-338.

Ke, S., Lin, P., Fan, H., Huang, H. and Zeng, X. (2013), "Variable-range-hopping conductivity in high-k Ba(Fe$_{0.5}$Nb$_{0.5}$)O$_3$ ceramics", *J. Appl. Phys.*, **114**(10), 104106-7.

Koops, C. (1951), "On the dispersion of resistivity and dielectric constant of some semiconductors at audio frequencies", *Phys. Rev.*, **83**(1), 121-124.

Kong, L.B., Zhang, T., Ma, J. and Boey, F. (2008), "Progress in synthesis of ferroelectric ceramic materials via high-energy mechanochemical technique", *Prog. Mater. Sci.*, **53**(2), 207-322.

Lee, D., Kim, M.G., Ryu, S., Jang, H.M. and Lee, S.G. (2005), "Epitaxially grown La-modified BiFeO$_3$ magnetoferroelectric thin films", *Appl. Phys. Lett.*, **86**(22), 222903-222905.

Li, G., Liu, S., Liao, F., Tian, S., Jing, X., Lin, J., Uesu, Y., Kohn, K., Saitoh, K., Terauchi, M., Di, N. and Cheng, Z. (2004a), "The structural and electric properties of the perovskite system BaTiO$_3$-Ba(Fe$_{1/2}$Ta$_{1/2}$)O$_3$", *J. Solid State Chem.*, **177**(4), 1695-1703.

Li, J., Wang, J., Wuttig, M., Ramesh, R., Wang, N., Ruette, B. and Pyatakov, A.P. (2004b), "Influence of Mn and Nb dopants on electric properties of chemical-solution-deposited BiFeO$_3$ films", *Appl. Phys. Lett.*, **84**(24), 5261-5263.

Mishra, A., Choudhary, S.N., Prasad, K., Choudhary, R.N.P. and Murthy, V.R.K. (2012), "Dielectric relaxation in complex perovskite Ba(Bi$_{1/2}$Ta$_{1/2}$)O$_3$", *J. Mater. Sci.: Mater. Electron.*, **23**(1), 185-192.

Patel, P.K., Yadav, K.L., Singh, H. and Yadav, A.K. (2014), "Origin of giant dielectric constant and magnetodielectric study in Ba(Fe$_{0.5}$Nb$_{0.5}$)O$_3$ nanoceramics", *J. Alloys Compd.*, **591**, 224-229.

Phatungthane, T., Rujijanagul, G., Pengpat, K., Eitssayeam, S., Tunkasiri, T., Cotica, L.F., Guo, R. and Bhalla, A.S. (2014), "Dielectric and impedance measurements on (1-x)Ba(Fe$_{1/2}$Ta$_{1/2}$)O$_3$-xBa(Zn$_{1/3}$Ta$_{2/3}$)O$_3$

ceramics", *Curr. Appl. Phys.*, **14**(12), 1819-1824.

Prasad, K., Bhagat, S., Amarnath, K., Choudhary, S.N. and Yadav, K.L. (2009), "Dielectric relaxation in lead-free perovskite Ba(Bi$_{1/2}$Nb$_{1/2}$)O$_3$", *Phys. Status Solidi A*, **206**(2), 316-320.

Prasad, K., Bhagat, S., Amarnath, K., Choudhary, S.N. and Yadav, K.L. (2010a), "Electrical conduction in Ba(Bi$_{0.5}$Nb$_{0.5}$)O$_3$ ceramic: Impedance spectroscopy analysis", *Mater. Sci. - Poland*, **28**(2009), 317-325.

Prasad, K., Chandra, K.P., Bhagat, S., Choudhary, S.N. and Kulkarni, A.R. (2010b), "Structural and electrical properties of lead-free perovskite Ba(Al$_{1/2}$Nb$_{1/2}$)O$_3$", *J. Amer. Ceram. Soc.*, **93**(1), 190-196.

Prasad, K., Lily, Kumari, K., Chandra, K.P., Yadav, K.L. and Sen, S. (2007a), "Electrical properties of a lead-free perovskite ceramic: (Na$_{0.5}$Sb$_{0.5}$)TiO$_3$", *Appl. Phys. A*, **88**(2), 377-383.

Prasad, K., Kumari, K. and Yadav, K.L. (2007b), "Hopping type of conduction in (Na$_{0.5}$Bi$_{0.5}$)ZrO$_3$ ceramic", *J. Phys. Chem. Solids*, **68**(8), 1508-1514.

Raevski, I., Prosandeev, S., Bogatin, A., Malitskaya, M. and Jastrabik, L. (2003), "High dielectric permittivity in AFe$_{1/2}$B$_{1/2}$O$_3$ nonferroelectric perovskite ceramics (A = Ba, Sr, Ca; B = Nb, Ta, Sb)", *J. Appl. Phys.*, **93**(7), 4130-4136.

Rebuffi, L., Troian, A., Ciancio, R., Carlino, E., Amimi, A., Leonardi, A. and Scardi, P. (2016), "On the reliability of powder diffraction Line Profile Analysis of plastically deformed nanocrystalline systems", *Sci. Rep.*, **6**, 20712-20724.

Sahoo, S.K., Agarwal, K., Singh, A.K., Polke, B.G. and Raha, K.C. (2010), "Characterization of γ- and α-Fe$_2$O$_3$ nano powders synthesized by emulsion precipitation-calcination route and rheological behaviour of α-Fe$_2$O$_3$", *Int. J. Engg. Sci. Technol.*, **2**(8), 118-126.

Sivasankaran, S., Sivaprasad, K., Narayanasamy, R. and Satyanarayana, P. (2011), "X-ray peak broadening analysis of AA 6061$_{100-x}$ - $x$wt.% Al$_2$O$_3$ nanocomposite prepared by mechanical alloying", *Mater. Char.*, **62**(7), 661-672.

Tickoo, R., Tandon, R., Bamzai, K. and Kotru, P. (2003), "Dielectric and piezoelectric characteristics of samarium modified lead titanate ceramics", *Mater. Sci. Eng.: B*, **103**(2), 145-151.

Tiwari, J.P. and Shahi, K. (2007), "Super-linear frequency dependence of ac conductivity of disordered Ag$_2$S-Sb$_2$S$_3$ at cryogenic temperatures", *Philos. Mag.*, **87**(29), 4475-4500.

Wang, Z., Chen, X.M., Ni, L. and Liu, X.Q. (2007a), "Dielectric abnormities of complex perovskite Ba(Fe$_{1/2}$Nb$_{1/2}$)O$_3$ ceramics over broad temperature and frequency range", *Appl. Phys. Lett.*, **90**(2), 022904-6.

Wang, Z., Chen, X.M., Ni, L., Liu, Y.Y. and Liu, X.Q. (2007b), "Dielectric relaxations in Ba(Fe$_{1/2}$Ta$_{1/2}$)O$_3$ giant dielectric constant ceramics", *Appl. Phys. Lett.*, **90**(10), 102905-102907.

OP